astronomy

CITESCORE
2.3

Article

Cosmological Viability of Linear and Power-Law Models in $f(T,B,\mathcal{T})$ Gravity Universe

Yahia Al-Omar, Majida Nahili and Nidal Chamoun

MDPI

https://doi.org/10.3390/astronomy5010005

astronomy

MDPI

Article

Cosmological Viability of Linear and Power-Law Models in $f(T,B,\mathcal{T})$ Gravity Universe

Yahia Al-Omar [1,*], Majida Nahili [1,2] and Nidal Chamoun [3,4,*]

[1] Department of Physics, Faculty of Sciences, Damascus University, Damascus P.O. Box 30621, Syria
[2] Faculty of Pharmacy, Syrian Private University, Damascus P.O. Box 36822, Syria
[3] Department of Statistics, Faculty of Sciences, Damascus University, Damascus P.O. Box 30621, Syria
[4] CASP, Antioch Syrian University, Maaret Saidnaya, Damascus, Syria
* Correspondence: yahia.alomar@damascusuniversity.edu.sy (Y.A.-O.); chamoun@uni-bonn.de (N.C.)

Abstract

We investigate the cosmological implications of torsion–boundary gravity with explicit matter coupling in $f(T,B,\mathcal{T})$ gravity. The purpose is to examine if such couplings offer observationally viable extensions to standard cosmology. Focusing on linear and power-law model realizations, we derive the modified Friedmann equations and analyze the resulting background dynamics. Using a combination of late-time datasets—including Cosmic Chronometers, Type Ia Supernovae, and Baryon Acoustic Oscillations—we perform a joint likelihood analysis to constrain the model parameters. Our results show that both $f(T,B,\mathcal{T})$ models remain compatible with current observations and effectively reduce to the ΛCDM paradigm in their appropriate parameter limits. While the power-law model exhibits mild dynamical deviations at intermediate redshifts, it remains statistically indistinguishable from the standard cosmological model. We conclude that $f(T,B,\mathcal{T})$ gravity represents a viable and robust extension of torsional modified gravity, motivating further study of non-minimal matter–geometry couplings in cosmology.

Keywords: observational constraints; $f(T,B,\mathcal{T})$ gravity; matter–geometry coupling

1. Introduction

The drive to understand how the universe began, what it is made of, and how it evolves continues to push us beyond General Relativity (GR). Although GR has been remarkably successful, it still faces challenges—such as explaining cosmic acceleration, resolving the Hubble tension, and uncovering the nature of dark energy. These open questions have encouraged the study of alternative theories, including modified Teleparallel Gravity, which describes gravity through spacetime torsion instead of curvature, offering a different geometric picture while remaining dynamically equivalent to GR [1–3].

In the Teleparallel Equivalent of General Relativity (TEGR), gravity is reformulated so that the tetrad field becomes the fundamental variable and torsion—not curvature—encodes gravitational effects. The torsion scalar T plays the role normally held by the Ricci scalar R, and the TEGR action reproduces Einstein's field equations exactly. Motivated by extending this framework, many studies have explored replacing T with an arbitrary function $f(T)$. These $f(T)$ models can drive late-time cosmic acceleration without dark energy and maintain second-order field equations, which has led to wide applications in areas such as cosmic acceleration [4–7], inflation [8,9], gravitational waves [10], and thermodynamics [11].

Received: 12 December 2025
Revised: 28 January 2026
Accepted: 5 February 2026
Published: 2 March 2026

However, pure $f(T)$ gravity typically breaks local Lorentz invariance and cannot [12] fully describe the connection between torsion and curvature. To overcome this limitation, the boundary term B was introduced, giving rise to the more general $f(T, B)$ gravity that unifies and extends both $f(T)$ and $f(R)$ theories. The inclusion of B adds theoretical flexibility and produces richer cosmological behavior in both early and late epochs. Recent observational analyses—using CMB distance priors [13], and low-redshift datasets [14]—show that $f(T, B)$ models remain compatible with current data, being further constrained at late times by $H(z)$ measurements [15] and at early times via Big Bang nucleosynthesis in extended formulations [16].

A broader class of Teleparallel Gravity emerges when the action depends explicitly on the trace of the energy–momentum tensor $\mathcal{T}$, introducing a direct coupling between matter and spacetime geometry. Following the idea of curvature-based $f(R, \mathcal{T})$ gravity [17], the teleparallel generalization $f(T, B, \mathcal{T})$ proposed in [18] unifies the torsion scalar T, the boundary term B, and the matter trace $\mathcal{T}$ within a single Lagrangian. This added flexibility leads to modified background dynamics and altered matter evolution, potentially leaving observable signatures in late-time cosmology. Such features make these models promising candidates for addressing tensions like the H_0 discrepancies [19], while also providing a well-motivated framework to explore nonminimal matter–geometry interactions using current data.

Recent studies further motivate this approach and demonstrate the constraining power of late-time data. Pantheon+ (2023) combined Type Ia Supernovae (SNe Ia), Cosmic Chronometers (CC), and Baryon Acoustic Oscillations (BAO) data to place stringent bounds on $f(T)$ models, showing they can produce diverse Hubble constant values, potentially easing late-time tensions [12]. Subsequent analyses using DESI BAO and DES SNe Ia (2024) find Bayesian preference for late-time $f(T)$ cosmologies over ΛCDM, with H_0 broadly consistent with local measurements [20]. Studies of $f(T, \mathcal{T})$ gravity (2024) show that late-time datasets constrain model parameters sensitively to H_0 priors, with BAO tending to lower inferred H_0 [21]. Recent work combining DESI, PantheonPlus, DESY5, and CMB data (2025) finds torsion parameters consistent with zero and derived H_0 and clustering values close to ΛCDM, indicating no strong evidence for large torsion effects [22]. Model-independent cosmographic analyses (DESI 2024) further highlight the precision of late-time data in testing deviations from standard cosmology [23].

In this work, we consider a phenomenological and partially speculative extension of torsional modified gravity, motivated by the Quintom paradigm, with the aim of illustrating how generalized gravitational dynamics may provide a unified framework relevant to both late-time cosmic acceleration and early-universe phenomena. This perspective is adopted not as a definitive alternative to ΛCDM, but as an exploratory framework to assess the viability and observational consequences of extended torsional dynamics under current and forthcoming cosmological data.

Motivated by recent developments, we employ Cosmic Chronometers [24–28], Type Ia Supernovae [29–32], and Baryon Acoustic Oscillations [30,33] to test two representative $f(T, B, \mathcal{T})$ gravity models. Focusing on linear and power-law forms, which range from minimal departures from TEGR to nonlinear, scale-dependent modifications, this combined analysis allows a data-driven assessment of whether torsion- and boundary-induced effects remain viable under precise late-time observations. By solving the modified Friedmann equations and constructing full likelihoods, we constrain the torsion, boundary, and matter-trace contributions using a comprehensive dataset that jointly maps the Hubble expansion across a wide redshift range.

This paper is organized as follows: in Section 2, we first introduce the theoretical framework of $f(T, B, \mathcal{T})$ gravity and then derive the cosmological field equations; in Section 3,

we briefly describe the observational datasets used—Cosmic Chronometers, Type Ia Supernovae, and Baryon Acoustic Oscillations—as well as the statistical methodology adopted to place bounds on the model parameters; in Section 4, we present the corresponding bounds, including best-fit values, confidence intervals, and comparisons with the standard ΛCDM cosmology; and finally, Section 5 summarizes the main results and states possible directions for future research within the framework of torsion-based modified gravity.

2. Cosmology in $f(T, B, \mathcal{T})$ Gravity

Teleparallel Gravity reformulates gravitation by identifying torsion, rather than curvature, as the fundamental agent of the gravitational interaction [34]. This framework is built upon the tetrad fields ${e^A}_\mu$, which define an orthonormal basis at each point in spacetime and connect the spacetime metric to the Minkowski metric via the relation:

$$g_{\mu\nu} = \eta_{AB} {e^A}_\mu {e^B}_\nu. \tag{1}$$

Gravitational dynamics are described using the curvature-free Weitzenböck connection, constructed directly from the tetrads:

$${\Gamma^\rho}_{\mu\nu} = e_A{}^\rho \partial_\nu {e^A}_\mu, \tag{2}$$

which gives rise to a non-vanishing torsion tensor:

$${T^\rho}_{\mu\nu} = {\Gamma^\rho}_{\nu\mu} - {\Gamma^\rho}_{\mu\nu}. \tag{3}$$

From the torsion tensor, one can define the contorsion tensor [35], measuring the difference between the Weitzenböck and Levi-Civita connections,

$${K^\rho}_{\mu\nu} = \frac{1}{2}\left({T_\mu}^\rho{}_\nu + {T_\nu}^\rho{}_\mu - {T^\rho}_{\mu\nu}\right), \tag{4}$$

and the superpotential,

$${S_\rho}^{\mu\nu} = \frac{1}{2}\left({K^{\mu\nu}}_\rho + \delta^\mu_\rho {T^{\alpha\nu}}_\alpha - \delta^\nu_\rho {T^{\alpha\nu}}_\alpha\right), \tag{5}$$

from which the torsion scalar, the central invariant of the theory, is constructed as follows:

$$T = {S_\rho}^{\mu\nu} {T^\rho}_{\mu v}. \tag{6}$$

The action of TEGR is then built from this scalar:

$$S_{\text{TEGR}} = \frac{1}{16\pi G}\int d^4x e T + S_m, \tag{7}$$

where $e = \det({e^A}_\mu) = \sqrt{-g}$. Variation of this action with respect to the tetrad produces field equations that are dynamically equivalent to Einstein's equations from General Relativity [35].

A straightforward modification is to generalize the action to an arbitrary function of the torsion scalar, giving rise to $f(T)$ gravity:

$$S_{f(T)} = \frac{1}{16\pi G}\int d^4x e f(T) + S_m, \tag{8}$$

which leads to second-order field equations [36], in contrast to the fourth-order equations of curvature-based $f(R)$ gravity.

This framework can be further extended by introducing the teleparallel boundary term B, defined as

$$B = \frac{2}{e}\partial_\mu(eT^\mu), \quad \text{with} \quad T^\mu = T^\nu{}_{\mu\nu}, \tag{9}$$

which satisfies the identity $R = -T + B$, thereby linking torsion and curvature and allowing a unified description of both geometric formulations [14], working with the metric signature $(+,-,-,-)$ and a vanishing spin connection. The resulting $f(T,B)$ gravity is described by the action:

$$S_{f(T,B)} = \frac{1}{16\pi G}\int d^4x e f(T,B) + S_m. \tag{10}$$

To introduce direct non-minimal coupling between matter and geometry, the action can be extended to depend also on the trace of the energy-momentum tensor, $\mathcal{T}$. The action for $f(T,B,\mathcal{T})$ gravity is as follows:

$$S = \frac{1}{2\kappa}\int d^4x e f(T,B,\mathcal{T}) + \int d^4x e\mathcal{L}_m. \tag{11}$$

Following [18] and restricting to our case of isotropic pressure, we vary this action with respect to the tetrad field to get the field equations (see Appendix A for technicalities):

$$\begin{aligned} &2e\delta^\lambda_\nu\Box f_B - 2e\nabla^\lambda\nabla_\nu f_B + eBf_B\delta^\lambda_\nu + 4e\left(\partial_\mu f_B + \partial_\mu f_T\right)S_\nu{}^{\mu\lambda} \\ &+4e^\alpha_\nu\partial_\mu\left(eS_\alpha{}^{\mu\lambda}\right)f_T - 4ef_T T^\sigma_{\mu\nu}S_\sigma{}^{\mu\lambda} - ef\delta^\lambda_\nu - 2ef_{\mathcal{T}}\left(e^\alpha_\nu\Theta^\lambda_\alpha + pe^\lambda_\nu\right) = \kappa^2 e\Theta^\lambda_\nu, \end{aligned} \tag{12}$$

where Θ^λ_ν is the matter energy-momentum tensor. Here and throughout, we employ the shorthand notation for partial derivatives: $f_T \equiv \partial f/\partial T$, $f_B \equiv \partial f/\partial B$, $f_{\mathcal{T}} \equiv \partial f/\partial\mathcal{T}$.

To apply this framework to cosmology, we consider a spatially flat FLRW universe with the metric $ds^2 = -dt^2 + a^2(t)\delta_{ij}dx^i dx^j$. For this geometry, the torsion scalar and boundary term take the simple forms:

$$T = -6H^2, \qquad B = -6(\dot{H} + 3H^2). \tag{13}$$

The first modified Friedmann equation is obtained from the time–time component ($\nu = \lambda = 0$) of the field Equation (12). For the perfect-fluid matter source and the FLRW tetrad, the contortion and superpotential terms simplify considerably. After substituting the relations (13) and evaluating the derivatives, one arrives at the energy constraint:

$$\kappa^2\rho = -3H^2(3f_B + 2f_T) - 3H\dot{f}_B + 3\dot{H}f_B + \frac{1}{2}f - \frac{1}{2e}f_{\mathcal{T}}(\rho + p). \tag{14}$$

This equation provides the basis for constructing cosmological models within the $f(T,B,\mathcal{T})$ framework and for confronting them with observational data.

We note that the explicit dependence on $\mathcal{T}$, in the gravitational Lagrangian, generally leads to a non-zero covariant divergence of the matter energy-momentum tensor, $\nabla_\mu\Theta^{\mu\nu} \neq 0$. In this work, which focuses on constraining the background expansion, we follow the common practice of assuming an approximate conservation, as in similar studies, by using the standard matter density ρ_m directly in the Friedmann equations [37].

3. Cosmological Datasets and Joint Analysis

To test the ability of our modified gravity model to reproduce the universe's expansion history, we use a multi-probe observational approach. Combining different datasets allows us to break degeneracies that would remain if each probe were used on its own, leading to more reliable constraints on the model parameters. Our analysis includes late-time expansion measurements from Cosmic Chronometers, the acoustic scale encoded in Baryon Acoustic Oscillations, and the luminosity–distance relation of Type Ia Supernovae. To-

gether, these datasets trace the expansion history across a wide redshift range and offer complementary information on the underlying cosmological dynamics.

Cosmic Chronometers directly measure the Hubble parameter through differential age estimates of passively evolving galaxies [38]. The relation

$$H(z) = -\frac{1}{1+z}\frac{dz}{dt} \tag{15}$$

arises from differentiating the definition of redshift with respect to cosmic time, making this method largely geometric and relatively insensitive to stellar-population assumptions. We use 46 uncorrelated CC measurements covering $0 < z < 2.36$ [39], one of the most comprehensive compilations currently available. These data provide a strong anchor for the expansion rate, especially at intermediate redshifts, and complement distance-based observations used in the joint analysis.

The distance–redshift relation is further constrained using Baryon Acoustic Oscillations and Type Ia Supernovae. BAO act as a standard ruler encoded in the large-scale clustering of galaxies, providing geometric information through both transverse and radial distance measurements. In our analysis, we use the comoving distance,

$$D_M(z) = c\int_0^z \frac{dz'}{H(z')}, \tag{16}$$

and the Hubble distance,

$$D_H(z) = \frac{c}{H(z)}, \tag{17}$$

both expressed relative to the sound horizon at the drag epoch, r_d.

We adopt the recent DESI 2024 BAO release [40], which reports high-precision measurements across the redshift range $(0.295 \lesssim z \lesssim 2.33)$. These measurements are derived from a combination of galaxy and quasar tracers, including bright galaxy samples (BGS) at low redshifts, luminous red galaxies (LRG) and emission-line galaxies (ELG) at intermediate redshifts, and quasars (QSO) and Lyman-α forest quasars (Lyα QSO) at high redshifts. Each tracer probes a distinct redshift interval and clustering regime, enabling DESI to robustly detect the BAO feature over a wide span of cosmic history.

Transverse distance measurements D_M/r_d and radial distance measurements D_H/r_d are obtained from the LRG, ELG, QSO, and Lyα QSO samples, while isotropic volume-averaged distances D_V/r_d are extracted from the low-redshift galaxy sample. The three distance measurements involve the product $r_d H$ revealing a degeneracy. In total, our analysis incorporates 12 independent BAO observables: five measurements of D_M/r_d, five measurements of D_H/r_d, and two measurements of D_V/r_d, together with their associated uncertainties and covariance information as provided by the DESI collaboration.

In our analysis, the BAO sound horizon (r_d) is fixed to the Planck 2018 value ($r_d = 147.05$ Mpc). This choice effectively imposes a CMB-informed prior, enabling the combination of BAO, CC, and SNe Ia to constrain (H_0) and the cosmological parameters. We note that with a fixed (r_d), the (r_d)–(H_0) degeneracy is broken by assumption rather than being independently resolved by late-time data. An alternative approach would be to leave (r_d) free or impose a BBN prior on $(\Omega_b h^2)$, which would propagate early-universe uncertainties into the late-time constraints.

For the distance ladder, we include the Pantheon+SH0ES compilation [41], consisting of 1701 uniformly calibrated Type Ia Supernovae. After applying the standard low-redshift cut $z > 0.01$ to mitigate the impact of local peculiar velocities, 1588 supernovae remain in the sample.

The supernova observables are expressed in terms of the distance modulus, defined as $\mu(z) \equiv m_B - M_B = 5\log_{10}[d_L(z)/\mathrm{Mpc}] + 25$, where m_B denotes the observed apparent peak magnitude in the rest-frame B-band, and M_B is the absolute magnitude of a fiducial Type Ia supernova. The apparent magnitude encodes the cosmological dependence through the luminosity distance,

$$d_L(z) = (1+z)D_M(z), \tag{18}$$

which is particularly sensitive to the expansion history at low and intermediate redshifts.

For the Pantheon+SH0ES dataset, the absolute magnitude is fixed to $M_B = -19.3$, following the SH0ES calibration. No additional host-galaxy mass-step parameter is introduced in our analysis, as host-mass corrections are already incorporated into the calibrated distance moduli. We make use of the full statistical and systematic covariance matrix provided by the Pantheon+SH0ES collaboration, ensuring a consistent propagation of observational uncertainties. This absolute calibration anchors the distance ladder and provides a powerful constraint on cosmological models that modify the late-time expansion rate, particularly through their impact on the inferred value of H_0.

To quantify consistency between theory and observations, we combine the individual likelihoods of CC, BAO, and SNe under the assumption of statistical independence:

$$\Phi^2_{\mathrm{joint}} = \Phi^2_{\mathrm{CC}} + \Phi^2_{\mathrm{BAO}} + \Phi^2_{\mathrm{SNe}}. \tag{19}$$

For the uncorrelated CC dataset, the chi-squared contribution is defined as

$$\Phi^2_{\mathrm{CC}} = \sum_i \frac{[H_{\mathrm{obs}}(z_i) - H_{\mathrm{th}}(z_i)]^2}{\sigma_i^2(z_i)}. \tag{20}$$

where $H_{\mathrm{obs}}(z_i)$ is the observed Hubble parameter at redshift z_i, $H_{\mathrm{th}}(z_i)$ is the theoretical prediction, and $\sigma_{\mathrm{i}}(z_i)$ is the corresponding measurement uncertainty. Correlated datasets, such as BAO and SNe, use the multivariate Gaussian form

$$\Phi^2 = (\mathrm{m}_{\mathrm{obs}} - \mathrm{m}_{\mathrm{th}})^{\intercal}\Sigma^{-1}(\mathrm{m}_{\mathrm{obs}} - \mathrm{m}_{\mathrm{th}}), \tag{21}$$

where $\mathrm{m}_{\mathrm{obs}}$ and m_{th} denote the vectors of observed and theoretically predicted observables, respectively, and Σ is the corresponding covariance matrix incorporating both statistical and systematic uncertainties.

We explore the parameter space using a Markov Chain Monte Carlo (MCMC) sampler, allowing us to map the full posterior distribution and capture correlations among parameters. The reduced chi-squared

$$\tilde{\chi}^2 = \frac{\Phi^2_{\mathrm{joint}}}{(N_{\mathrm{data}} - N_{\mathrm{parameters}})} \tag{22}$$

provides an overall assessment of the model's performance, with values near unity indicating a satisfactory fit to the combined data. This joint (CC+BAO+SNe) analysis provides a robust and coherent test of the modified gravity model across cosmic history.

In general, the reduced chi-squared $\tilde{\chi}^2$ provides a dimensionless measure of how well a model describes the data per degree of freedom. Values near unity indicate good agreement with the reported uncertainties, while significantly larger values suggest a poor fit or underestimated errors. Substantially smaller values can reflect conservative error estimates/residual correlations, at times fitting noise rather than signal, but they also indicate that the model describes the data very closely. In all cases, $\tilde{\chi}^2$ serves as a useful diagnostic for the overall consistency between theoretical predictions and observations.

Beyond goodness-of-fit, we assess the relative performance of competing cosmological models using information criteria that penalize model complexity. In particular, we employ the Akaike Information Criterion (AIC) and the Bayesian Information Criterion (BIC), defined, respectively, as

$$\mathrm{AIC} = \chi^2_{\min} + 2k, \qquad \mathrm{BIC} = \chi^2_{\min} + k \ln N, \tag{23}$$

where k is the number of free parameters and N is the total number of data points. Here, $\chi^2_{\min}$ denotes the minimum chi-squared value achieved at the best-fit parameters, representing the absolute goodness-of-fit of the model. Both criteria balance the quality of the fit against the number of model parameters, thereby disfavoring overly complex models that do not yield a commensurate improvement in likelihood.

4. Cosmological Models and Results

This section, divided by subheadings, should provide a concise and precise description of the experimental results, their interpretation, and the experimental conclusions that can be drawn.

4.1. The Linear Model

A natural starting point for exploring extended Teleparallel Gravity is the minimal linear form:

$$f(T, B, \mathcal{T}) = \alpha T + \beta B + \gamma \mathcal{T}. \tag{24}$$

This choice keeps the theory analytically transparent while capturing the main features of $f(T, B, \mathcal{T})$ framework. Each term plays a distinct role: α rescales the standard TEGR Lagrangian, the βB encodes the torsion–curvature relation (as previously examined in linear $f(T, B)$ models [42]), and $\gamma\mathcal{T}$ introduces a matter–geometry coupling similar to the linear $f(T, \mathcal{T})$ model of ref. [37].

Despite its simplicity, this linear model provides a clean and physically motivated baseline from which the effects of the additional degrees of freedom can be systematically studied. It also unifies several cornerstone theories as limiting cases: TEGR is recovered for $\beta = \gamma = 0$, GR emerges for $\alpha = -\beta$ and $\gamma = 0$, and the standard GR limit corresponds to $\alpha = -\beta = 1$. In this last case, a non-zero γ becomes the only genuinely new parameter driving deviations from the GR expansion history.

For cosmological applications, we specialize to a spatially homogeneous and isotropic universe, described by the Friedmann–Lemaître–Robertson–Walker (FLRW) metric. In this background, the matter and radiation components evolve according to their standard conservation equations. The total energy density can therefore be written as $\rho(z) = \rho_{m0}(1+z)^3 + \rho_{r0}(1+z)^4$, where ρ_{m0} and ρ_{r0} denote the present-day matter and radiation densities, respectively. The pressure is dominated by the relativistic component and takes the form of $p(z) = \frac{1}{3}\rho_{r0}(1+z)^4$, while the trace of the energy–momentum tensor becomes $\mathcal{T}(z) = \rho_{m0}(1+z)^3$, reflecting the fact that only the pressureless matter sector contributes to $\mathcal{T}$. For the FLRW geometry, the tetrad determinant reads $e = a^3 = (1+z)^{-3}$. Moreover, time derivatives can be expressed in terms of redshift through the relation $\frac{d}{dt} = -(1+z)H\frac{d}{dz}$.

The background dynamics of the model are governed by a modified Friedmann Equation (14), which is conveniently expressed in terms of the dimensionless Hubble parameter $E(z) = H(z)/H_0$. For the linear realization of the theory under consideration, the modified expansion law takes the form

$$\frac{dE}{dz} = \frac{1}{2\beta(1+z)}\left[\frac{\mathcal{A}(z) + \mathcal{G}(z)}{E} + (6\beta + 3\alpha)E\right], \tag{25}$$

where $\mathcal{A}(z) = \Omega_{m0}(1+z)^3 + \Omega_{r0}(1+z)^4$ encodes the standard matter and radiation contributions, and $\mathcal{G}(z) = \frac{\gamma}{6}\left[\Omega_{m0}(1+z)^3 + 3\Omega_{m0}(1+z)^6 + 4\Omega_{r0}(1+z)^7\right]$.

Owing to the boundary nature of B, the coefficients α and β enter Equation (25) only through specific linear combinations, leading to a degeneracy in the linear sector of the modified Friedmann equation. As a result, cosmological observables constrain only the dynamically relevant combination appearing in the expansion law. To ensure numerical stability, the parameter estimation is therefore performed in a non-degenerate basis, with α and β reconstructed as derived parameters. The elongated confidence regions in the (α, β) plane thus reflect the intrinsic boundary-term redundancy of the theory.

Equation (25) provides the basis for our numerical integration of the expansion history and allows us to confront the linear model with late-time cosmological probes, including Cosmic Chronometers (Figure 1), Type Ia Supernovae (Figure 2), and their joint constraints together with BAO (Figure 3). The statistical inference of the model parameters is carried out within a Bayesian framework.

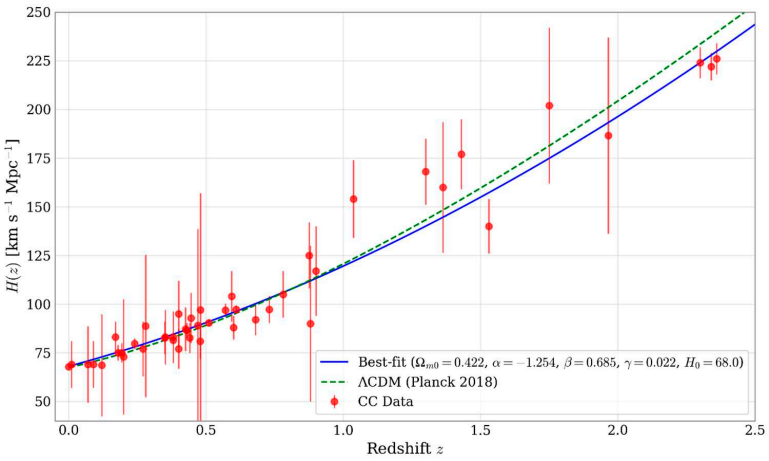

Figure 1. Best-fit $H(z)$ for the linear model (solid blue) compared with Planck 2018 ΛCDM (dashed green) and cosmic chronometer measurements (red points).

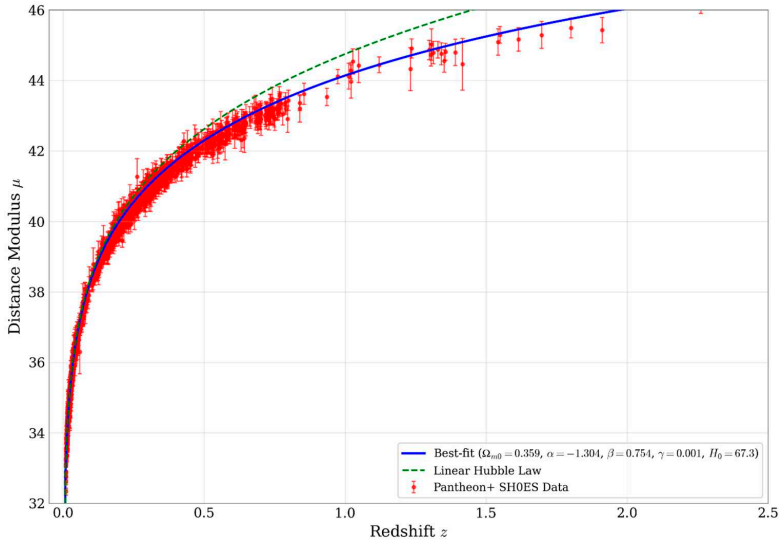

Figure 2. Distance modulus $\mu(z)$ for the linear model compared with Pantheon+SH0ES. The blue curve shows the best-fit prediction, the dashed green curve demonstrates the linear Hubble law, and the red points represent the observational data.

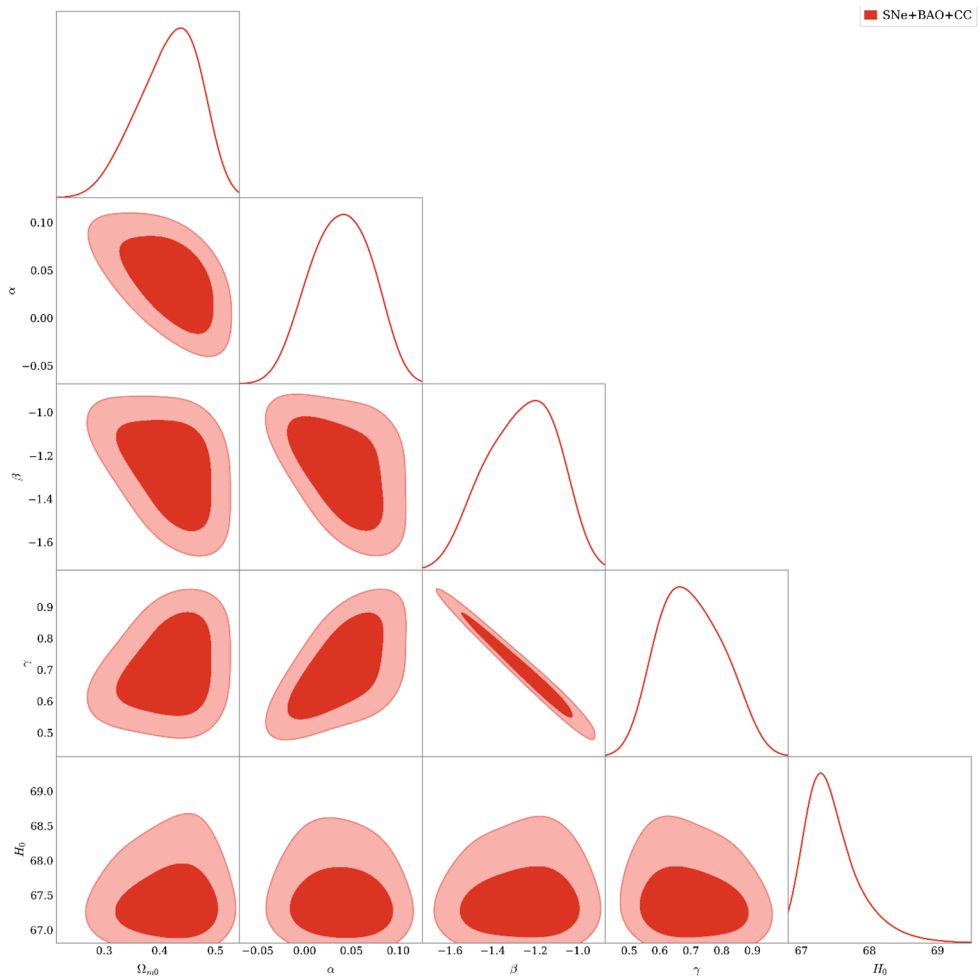

Figure 3. Posterior distributions and parameter covariances for the linear model from the joint SNe Ia + BAO + CC analysis. The contours show the 68% and 95% confidence regions.

We employ the affine-invariant ensemble Markov Chain Monte Carlo sampler implemented in the emcee package, using 50 walkers and 20,000 steps per walker. Convergence of the chains is assessed through the integrated autocorrelation time, complemented by a conservative burn-in removal corresponding to three times the maximum autocorrelation time, appropriate thinning, and visual inspection of the parameter trajectories. The Gelman–Rubin statistic $(\hat{R})$ is not adopted in this analysis, as it is primarily designed for multiple independent Markov chains rather than ensemble-based samplers.

For the Bayesian analysis, we adopt uniform priors on the Hubble constant and the present-day matter density parameter, specifically $H_0 \in [60, 80]$ kms^{-1}Mpc^{-1} and $\Omega_{m0} \in [0.1, 0.5]$, which allow the data to fully determine their preferred values while avoiding unphysical regions. The remaining parameters α, β, and γ are also assigned uniform priors over sufficiently broad intervals to encompass all physically plausible values, ensuring that the posterior distributions are primarily informed by the observational data rather than the prior assumptions. The resulting bounds on the parameter set $\{\alpha, \beta, \gamma, H_0, \Omega_{m0}\}$ are summarized in Table 1.

Throughout this analysis, the radiation density parameter is fixed to the Planck 2018 value, Ω_{r0}, as reported in the final cosmological parameter results of ref. [2]. This choice avoids degeneracies in the radiation sector and is standard practice in late-time cosmological reconstructions.

Table 1. Best-fit parameters for the linear model from different cosmological probes.

Dataset	Ω_{m0}	α	β	γ	H_0
SNe	$0.359^{+0.097}_{-0.104}$	$-1.304^{+0.200}_{-0.195}$	$0.754^{+0.141}_{-0.148}$	$0.001^{+0.067}_{-0.068}$	$67.33^{+0.55}_{-0.25}$
CC	$0.422^{+0.055}_{-0.076}$	$-1.254^{+0.178}_{-0.217}$	$0.686^{+0.133}_{-0.111}$	$0.022^{+0.045}_{-0.041}$	$68.03^{+1.01}_{-0.70}$
Joint	$0.426^{+0.051}_{-0.068}$	$-1.244^{+0.168}_{-0.207}$	$0.691^{+0.131}_{-0.102}$	$0.040^{+0.036}_{-0.036}$	$67.33^{+0.48}_{-0.24}$

The parameter constraints reveal notable trends. The matter density parameter Ω_{m0} shows variation between datasets, with the SNe-only analysis preferring a lower value near 0.35, while the CC and joint analyses converge with a higher value around 0.42.

The gravitational parameters α and β exhibit a consistent pattern: α is constrained to be negative, with values around -1.25 to -1.30, while β is positive, with values around 0.69–0.75. This specific relationship between α and β is essential for the model to satisfy the cosmological constraints. The matter–geometry coupling parameter γ is consistently small across all datasets, with its 1σ uncertainty ranges encompassing zero. This indicates that while a mild positive coupling is allowed by the data, a model with no direct coupling ($\gamma = 0$) remains statistically consistent with observations. The Hubble constant H_0 is measured to be approximately 67.3–68.0 km s^{-1} Mpc^{-1} across the datasets, showing strong consistency and alignment with Planck CMB measurements.

The overall quality of the fit is excellent, with total chi-squared values of $\chi^2_{\rm min} = 316.11$ (SNe), 24.25 (CC), and 356.58 (combined), corresponding to reduced values $\widetilde{\chi}^2 \simeq 0.20$, 0.59, and 0.22, respectively. The information criteria yield $(\mathrm{AIC}, \mathrm{BIC}) = (326.11, 352.96)$ for SNe, $(34.25, 43.39)$ for CC, and $(366.58, 393.61)$ for the joint analysis. These results indicate that the linear model provides an excellent fit to the data, reproducing a ΛCDM-like expansion history, with the matter–geometry coupling γ remaining consistent with zero and the $\alpha - \beta$ combination being tightly constrained.

4.2. The Power-Law Model

To extend the scope of the linear model and capture richer torsional dynamics, we consider the more general power-law form:

$$f(T, B, \mathcal{T}) = \widetilde{\alpha}(-T)^n + \widetilde{\beta}B + \widetilde{\gamma}\mathcal{T}. \tag{26}$$

This model introduces a nonlinear dependence on the torsion scalar, allowing the theory to generate late-time cosmic acceleration through purely geometric contributions rather than an explicit cosmological constant. The parameter $\widetilde{\alpha}$ controls the amplitude of the nonlinear torsion term, $\widetilde{\beta}$ retains the usual connection to the boundary term familiar from linear $f(T, B)$ gravity [43], and $\widetilde{\gamma}$ provides a matter–geometry coupling similar to that considered in $f(T, \mathcal{T})$ extensions [44].

The modified background evolution can again be written in terms of the $E(z)$, leading to the first-order differential equation:

$$\frac{dE}{dz} = \frac{1}{2\widetilde{\beta}(1+z)} \left\{ \frac{\mathcal{A}(z) + \widetilde{\mathcal{G}}(z)}{E} + \left(6\widetilde{\beta} + (2n+1)\widetilde{\alpha}(6H_0^2)^{n-1}E^{2(n-1)} \right) E \right\}, \tag{27}$$

where $\widetilde{\mathcal{G}}(z) = \frac{\widetilde{\gamma}}{6}\left[\Omega_{m0}(1+z)^3 + 3\Omega_{m0}(1+z)^6 + 4\Omega_{r0}(1+z)^7\right]$.

Equation (27) forms the basis of our numerical analysis and highlights the key difference from the linear case: the presence of a torsion-driven correction proportional to $E^{2(n-1)}$, which allows the model to interpolate between TEGR-like behavior and a wider family of modified-gravity cosmologies depending on the value of the exponent n.

Bayesian inference is performed using the affine-invariant sampler emcee with 60 walkers and 25,000 steps per walker, applying conservative burn-in removal and thinning based on the integrated autocorrelation time; visual inspection ensures chain convergence. Uniform priors are adopted for all parameters, with $H_0 \in [60, 80]$ kms^{-1}Mpc^{-1} and $\Omega_{m0} \in [0.1, 0.5]$, while $\tilde{\alpha}, \tilde{\beta}, \tilde{\gamma}$, and n are allowed wide, physically plausible ranges.

We test the power-law model against late-time probes—CC (Figure 4), SNe Ia (Figure 5), and the joint analysis (Figure 6)—with the resulting constraints on $\left\{\tilde{\alpha}, \tilde{\beta}, \tilde{\gamma}, n, H_0, \Omega_{m0}\right\}$ summarized in Table 2.

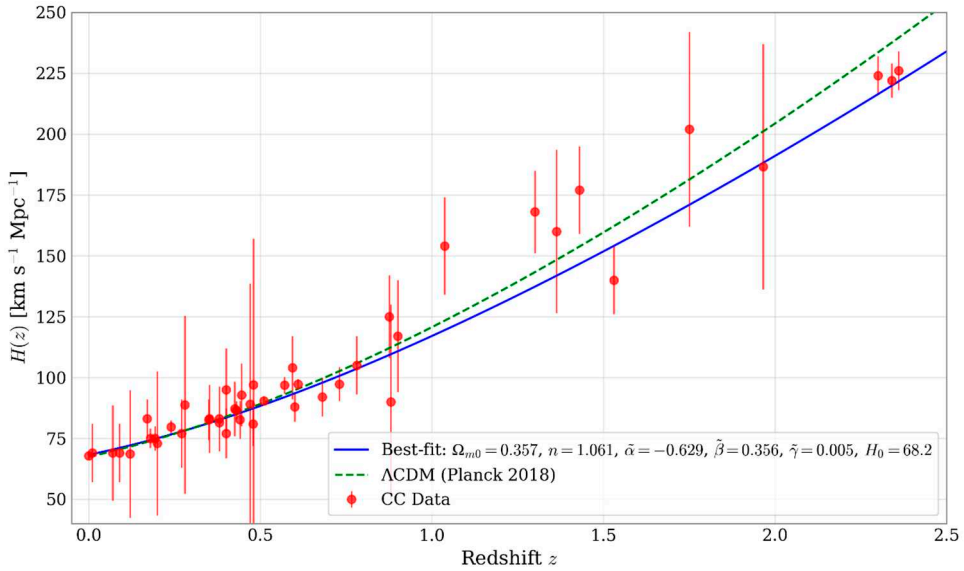

Figure 4. Best-fit $H(z)$ for the power-law model (solid blue) compared with Planck 2018 ΛCDM (dashed green) and cosmic chronometer measurements (red points).

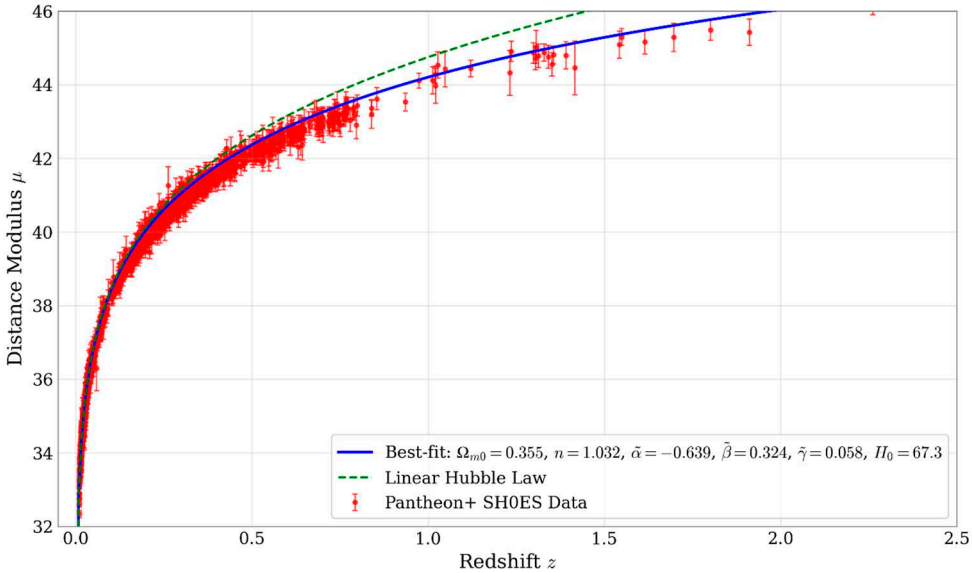

Figure 5. Distance modulus $\mu(z)$ for the power-law model compared with Pantheon+SH0ES. The blue curve shows the best-fit prediction, the dashed green curve is the linear Hubble law, and the red points represent the observational data.

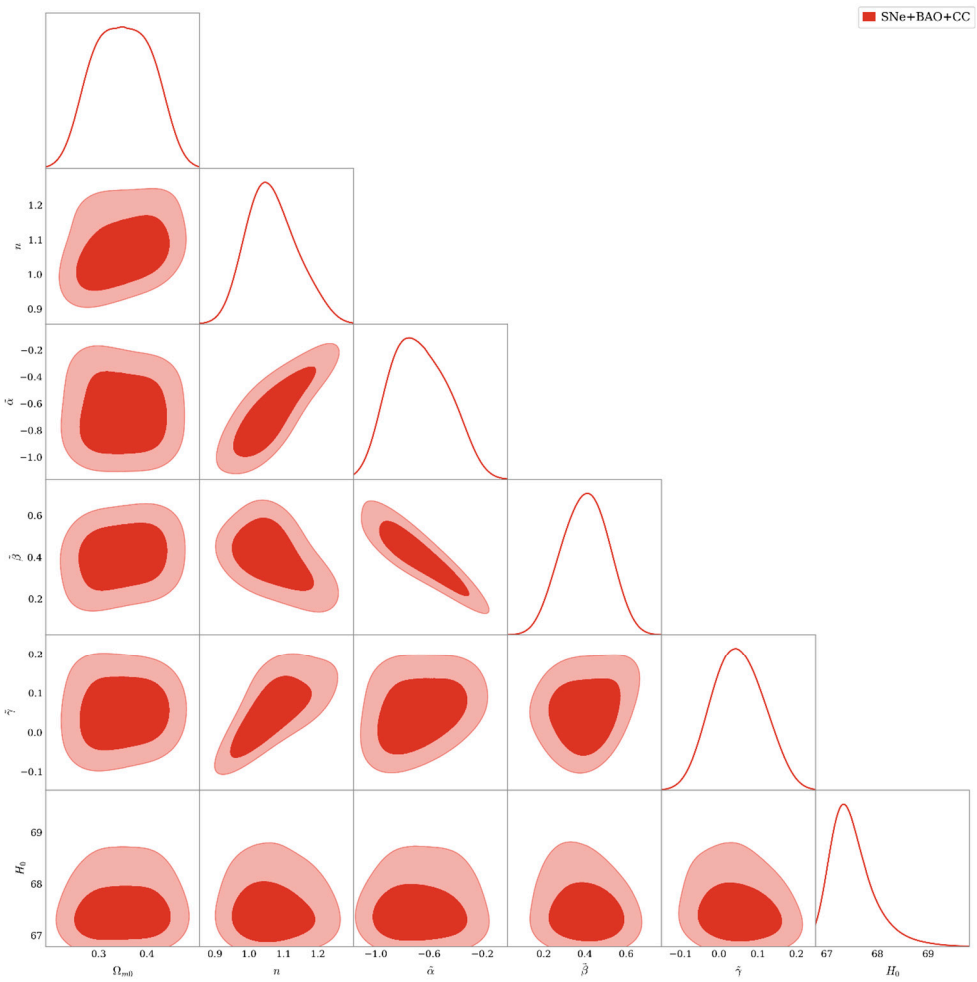

Figure 6. Posterior distributions and parameter covariances for the power-law model from the joint SNe Ia + BAO + CC analysis. The contours show the 68% and 95% confidence regions.

Table 2. Best-fit parameters for the power-law model from different cosmological probes.

Dataset	Ω_{m0}	n	$\widetilde{\alpha}$	$\widetilde{\beta}$	$\widetilde{\gamma}$	H_0
SNe	$0.355^{+0.064}_{-0.071}$	$1.032^{+0.137}_{-0.138}$	$-0.639^{+0.229}_{-0.227}$	$0.324^{+0.221}_{-0.157}$	$0.058^{+0.099}_{-0.107}$	$70.54^{+2.76}_{-3.01}$
CC	$0.357^{+0.067}_{-0.067}$	$1.061^{+0.097}_{-0.077}$	$-0.629^{+0.249}_{-0.255}$	$0.356^{+0.133}_{-0.132}$	$0.005^{+0.096}_{-0.070}$	$67.83^{+1.22}_{-1.27}$
Joint	$0.350^{+0.069}_{-0.069}$	$1.059^{+0.086}_{-0.064}$	$-0.692^{+0.267}_{-0.217}$	$0.409^{+0.108}_{-0.125}$	$0.047^{+0.073}_{-0.064}$	$68.27^{+1.07}_{-1.02}$

The constraints reveal several key features of the power-law model. The matter density parameter Ω_{m0} is consistently measured to be $\Omega_{m0} \approx 0.35$–0.36 across all datasets, in good agreement with Planck. The parameter n, which governs the deviation from a linear torsion scalar term, is consistently very close to one across all datasets, with a best-fit value of approximately 1.06. This suggests that the data do not strongly favor a significant power-law deviation from the linear TEGR limit ($n = 1$). This proximity to the linear limit ($n = 1$) indicates that, within current observational uncertainties, the power-law model effectively approaches the linear realization at the background level, reflecting the strong observational preference for ΛCDM-like expansion histories.

The parameter $\widetilde{\alpha}$ is consistently negative, with a central value around -0.64, while $\widetilde{\beta}$ is consistently positive, with a central value around 0.38. The matter–geometry coupling parameter $\widetilde{\gamma}$ is consistently found to be positive but very small, with its 1σ uncertainty range encompassing zero in all cases. This indicates that while a small coupling is mildly

preferred by the data, a model with no direct coupling ($\widetilde{\gamma} = 0$) is statistically consistent with the observations. The Hubble constant H_0 shows strong consistency across all datasets. All three analyses—SNe, CC, and joint—yield values within the narrow range of 67.4–68.2 km/s/Mpc, with small uncertainties, and align with the value inferred from Planck CMB measurements.

Statistically, the model provides an adequate fit to the data, with total chi-squared values $\chi^2_{\rm min} = 316.14$ (SNe), 23.05 (CC), and 357.09 (combined), corresponding to reduced values $\widetilde{\chi}^2 \simeq 0.20$, 0.56, and 0.21, respectively. When penalizing for model complexity, the information criteria yield $(\mathrm{AIC}, \mathrm{BIC}) = (326.14, 353.00)$ for SNe, $(33.05, 42.20)$ for CC, and $(367.09, 394.12)$ for the joint dataset. Overall, the power-law model fits the data well, with n close to unity and $\widetilde{\gamma}$ consistent with zero, effectively reproducing a ΛCDM-like expansion while remaining statistically competitive with the linear case.

5. Discussion

In this work, we have conducted a thorough investigation of the cosmological dynamics within the framework of $f(T, B, \mathcal{T})$ gravity, a theory that generalizes Teleparallel Gravity by incorporating both a boundary term B and the trace of the matter energy-momentum tensor $\mathcal{T}$. To navigate the complexity of this generalized theory, we proposed and constrained two specific, well-motivated models: a minimal linear model and a more general power-law extension.

The linear model, $f(T, B, \mathcal{T}) = \alpha T + \beta B + \gamma \mathcal{T}$, served as a transparent baseline. Our observational analysis, utilizing a combination of SNe, BAO, and CC data, revealed that the data are consistent with a non-zero matter–geometry coupling ($\gamma > 0$), although a model without such a coupling ($\gamma = 0$) remains within the statistical uncertainties. The constraints consistently pointed to a specific relationship between the gravitational parameters, with α negative and β positive, a necessary condition for the model to align with the observed expansion history.

The power-law model, $f(T, B, \mathcal{T}) = \widetilde{\alpha}(-T)^n + \widetilde{\beta} B + \widetilde{\gamma}\mathcal{T}$, was introduced to test for deviations beyond the linear regime. A key result is that the power-law index n is constrained to be very close to unity across all datasets. This strongly suggests that the current cosmological data do not favor a significant deviation from a linear torsion scalar term, effectively pulling this generalized model back towards the linear case and the TEGR limit. Similarly to the linear model, the parameters $\widetilde{\alpha}$ and $\widetilde{\beta}$ exhibit a consistent sign flip (negative and positive, respectively), and the coupling parameter $\widetilde{\gamma}$ is, again, consistent with zero within its confidence intervals.

The Hubble constant H_0 inferred from both models aligns closely with Planck values, showing consistency with early-universe measurements. However, the matter density parameter Ω_{m0} shows a notable difference: the power-law model yields $\Omega_{m0} \approx 0.35$, in close agreement with Planck, while the linear model consistently gives a higher value of $\Omega_{m0} \approx 0.36$–0.43. This divergence in the inferred matter content highlights the distinct ways in which the two parameterizations reconcile the geometric modifications with the observed expansion history, even as both provide excellent fits to the late-time data.

The overarching conclusion from our analysis of both models is two-fold. First, the inclusion of the boundary term B is crucial, as evidenced by the tightly constrained, non-trivial relationship between α and β (or $\widetilde{\alpha}$ and $\widetilde{\beta}$), which is distinct from both TEGR and GR. Second, while the data allow for a small, positive matter–geometry coupling governed by γ (or $\widetilde{\gamma}$), they do not require it. The fact that γ is consistent with zero in our most robust joint analysis indicates that the current late-time cosmological observations can be

well-explained by the geometric terms alone, without the need for a direct non-minimal coupling to $\mathcal{T}$.

In summary, $f(T, B, \mathcal{T})$ gravity provides a rich framework for modifying gravity. Our study demonstrates that its simplest manifestations are phenomenologically viable and can be tightly constrained by observations. Future work, incorporating a full linear perturbation analysis and a wider array of precision data, will be essential to further test the stability and viability of these models. Specifically, calculating the evolution of linear cosmological perturbations, the effective gravitational coupling G_{eff}, and the growth rate $f\sigma_8$ for the parameter ranges favored by our background analysis will determine if these models are also consistent with large-scale structure observations from galaxy clustering and weak lensing. Such an analysis will definitely establish whether the intriguing coupling between geometry and matter in the $f(T, B, \mathcal{T})$ framework plays a fundamental role in the evolution of both the cosmic expansion and structure formation.

Looking ahead, the implications of future high-precision surveys can provide further guidance on the relevance of these models. If forthcoming observations, such as DESI or Euclid, reveal a significant crossing of the phantom divide, models with dynamical dark energy—like Quintom-inspired or non-minimally coupled frameworks—would become especially compelling. The power-law $f(T, B, \mathcal{T})$ realization discussed here represents a minimal and observationally consistent example of such a scenario. Conversely, even if future data continue to favor a ΛCDM-like expansion, Quintom-inspired and non-minimally coupled frameworks remain valuable for exploring early-universe physics, offering a flexible theoretical laboratory to study deviations from standard cosmology across different epochs.

Author Contributions: Y.A.-O.: conceptualization, methodology, software, writing—original draft preparation; M.N.: supervision; N.C.: supervision, validation, writing—reviewing and editing. All authors have read and agreed to the published version of the manuscript.

Funding: This research received no external funding.

Data Availability Statement: The data supporting the findings of this study are available within the article. The authors acknowledge the use of publicly accessible cosmological data from the Planck 2018 Legacy Archive and preprints hosted on arXiv.

Acknowledgments: N.C. acknowledges support from the PIFI-CAS fellowship and from the Humboldt Foundation.

Conflicts of Interest: The authors declare no conflicts of interest.

Appendix A. Useful Formulae

We state below some formulae which prove to be useful when carrying out the variation with respect to the tetrad fields. For details of the derivation, one can consult [45].

With E_a^μ representing the inverse tetrad field ($E_m^\nu e_\mu^m = \delta_\mu^\nu$), we have the following equations:

$$\delta g^{\mu\nu} = -\left(g^{\nu\lambda} E_a^\mu + g^{\mu\lambda} E_a^\nu\right)\delta e_\lambda^a, \tag{A1}$$

$$\delta e = e E_a^\lambda \delta e_\lambda^a, \tag{A2}$$

$$e\delta T = e\left(\frac{1}{4}\delta\left(T^{\mu\nu\lambda}T_{\mu\nu\lambda}\right) + \frac{1}{2}\delta\left(T^{\mu\nu\lambda}T_{\nu\mu\lambda}\right) - \delta\left(T^\mu T_\mu\right)\right), \tag{A3}$$

$$\delta E_m^\sigma = -E_n^\sigma E_m^\mu \delta e_\mu^n,\ \partial_\nu E_m^\sigma = -E_n^\sigma E_m^\mu \partial_\nu e_\mu^n, \tag{A4}$$

$$\delta T_{\mu\nu}^\lambda = -E_a^\lambda T_{\mu\nu}^\beta \delta e_\beta^a + E_a^\lambda\left(\partial_\mu \delta e_\nu^a - \partial_\nu \delta e_\mu^a\right), \tag{A5}$$

$$\delta T^{\mu} = -\left(E_a^{\mu}T^{\lambda} + g^{\mu\lambda}T_a + T_a^{\lambda\mu}\right)\delta e_{\lambda}^{\alpha} + g^{\mu\nu}E_a^{\lambda}(\partial_{\lambda}\delta e_{\nu}^{a} - \partial_{\nu}\delta e_{\lambda}^{a}), \tag{A6}$$

$$\delta\left(T_{\mu}T^{\mu}\right) = -2\left(T^{\beta}T^{\alpha}{}_{\beta\mu} + T^{\alpha}T_{\mu}\right)E_a^{\mu}\delta e_{\alpha}^{a} + 2\left(T^{\alpha}E_a^{\mu} - T^{\mu}E_a^{\alpha}\right)\partial_{\alpha}\delta e_{\mu}^{a}, \tag{A7}$$

$$\delta\left(T_{\alpha\mu\nu}T^{\alpha\mu\nu}\right) = -4T^{\alpha\mu\nu}T_{\alpha\mu\beta}E_a^{\beta}\delta e_{\nu}^{a} + 4T_{\alpha}{}^{\mu\nu}E_a^{\alpha}\partial_{\mu}\delta e_{\nu}^{a}. \tag{A8}$$

From the above expressions, one can compute the variations of T and of $\left(B = \frac{2}{e}\partial_{\mu}(eT^{\mu})\right)$ in terms of δe_{ν}^{a} in order to get the field equations.

References

1. Perivolaropoulos, L.; Skara, F. Challenges for ΛCDM: An Update. *New Astron. Rev.* **2022**, *95*, 101659. [CrossRef]
2. Aghanim, N.; Akrami, Y.; Ashdown, M.; Aumont, J.; Baccigalupi, C.; Ballardini, M.; Banday, A.J.; Barreiro, R.B.; Bartolo, N.; Basak, S.; et al. Planck 2018 Results—VI. Cosmological Parameters. *Astron. Astrophys.* **2020**, *641*, A6. [CrossRef]
3. Velten, H.; Gomes, S.; Busti, V.C. Gauging the Cosmic Acceleration with Recent Type Ia Supernovae Data Sets. *Phys. Rev. D* **2018**, *97*, 083516. [CrossRef]
4. Bahamonde, S.; Dialektopoulos, K.F.; Hohmann, M.; Said, J.L.; Pfeifer, C.; Saridakis, E.N. Perturbations in Non-Flat Cosmology for $f(T)$ Gravity. *Eur. Phys. J. C* **2023**, *83*, 193. [CrossRef]
5. Hu, Y.M.; Zhao, Y.; Ren, X.; Wang, B.; Saridakis, E.N.; Cai, Y.F. The Effective Field Theory Approach to the Strong Coupling Issue in $f(T)$ Gravity. *J. Cosmol. Astropart. Phys.* **2023**, *2023*, 060. [CrossRef]
6. Koussour, M.; Altaibayeva, A.; Bekov, S.; Holmurodov, F.; Muminov, S.; Rayimbaev, J. Exploring Cosmological Evolution and Constraints in $f(T)$ Teleparallel Gravity. *Phys. Dark Universe* **2024**, *46*, 101664. [CrossRef]
7. Verma, S.; Dixit, A.; Pradhan, A.; Barak, M.S. Testing $f(T)$ Gravity with Cosmological Observations: Confronting the Hubble Tension and Implications for the Late-Time Universe. *J. High Energy Astrophys.* **2026**, *49*, 100440. [CrossRef]
8. Chakrabortty, M.; Sk, N.; Sanyal, S.; Sanyal, A.K. Inflation with $f(T)$ Teleparallel Gravity. *Eur. Phys. J. Plus* **2021**, *136*, 1213. [CrossRef]
9. Awad, A.; El Hanafy, W.; Nashed, G.G.L.; Odintsov, S.D.; Oikonomou, V.K. Constant-Roll Inflation in $f(T)$ Teleparallel Gravity. *J. Cosmol. Astropart. Phys.* **2018**, *2018*, 026. [CrossRef]
10. Nunes, R.C.; Pan, S.; Saridakis, E.N. New Observational Constraints on $f(T)$ Gravity through Gravitational-Wave Astronomy. *Phys. Rev. D* **2018**, *98*, 104055. [CrossRef]
11. Karami, K.; Abdolmaleki, A. Generalized Second Law of Thermodynamics in $f(T)$ Gravity. *J. Cosmol. Astropart. Phys.* **2012**, *2012*, 007. [CrossRef]
12. Briffa, R.; Escamilla-Rivera, C.; Said, J.L.; Mifsud, J. Constraints on $f(T)$ Cosmology with Pantheon+. *Mon. Not. R. Astron. Soc.* **2023**, *522*, 6024–6034. [CrossRef]
13. Chokyi, K.K.; Chattopadhyay, S. Cosmological Models within $f(T, B)$ Gravity in a Holographic Framework. *Particles* **2024**, *7*, 856–878. [CrossRef]
14. Briffa, R.; Escamilla-Rivera, C.; Said, J.L.; Mifsud, J. (T, B) Gravity in the Late Universe in the Context of Local Measurements. *Phys. Dark Universe* **2023**, *39*, 101153. [CrossRef]
15. Shekh, S.H.; Myrzakulov, N.; Bouali, A.; Pradhan, A. (T, B) Gravity with Statistically Fitting of $H(z)$. *Commun. Theor. Phys.* **2023**, *75*, 095401. [CrossRef]
16. Sultan, A.M.; Ali, M.; Rani, S.; Azhar, N.; Myrzakulov, N.; Shaymatov, S. Constraining Big Bang Nucleosynthesis in $f(T, B, T\_G, B\_G)$ Gravity. *Nucl. Phys. B* **2025**, *1018*, 117023. [CrossRef]
17. Carvalho, G.A.; Dos Santos, S.I.; Moraes, P.H.R.S.; Malheiro, M. Strange Stars in Energy–Momentum-Conserved $f(R, T)$ Gravity. *Int. J. Mod. Phys. D* **2020**, *29*, 2050075. [CrossRef]
18. Das, K.P.; Debnath, U. Anisotropic Strange Stars in Extended $f(T,B,\mathcal{T})$ Gravity with Electromagnetic Field. *Chin. J. Phys.* **2024**, *88*, 439–461. [CrossRef]
19. Nunes, R.C. Structure Formation in $f(T)$ Gravity and a Solution for H_0 Tension. *J. Cosmol. Astropart. Phys.* **2018**, *2018*, 052. [CrossRef]
20. Escamilla-Rivera, C.; Sandoval-Orozco, R. (T) Gravity after DESI Baryon Acoustic Oscillation and DES Supernovae 2024 Data. *J. High Energy Astrophys.* **2024**, *42*, 217–221. [CrossRef]
21. Duchaniya, L.K.; Mishra, B. Late Time Phenomena in $f(T, \mathcal{T})$ Gravity Framework: Role of H_0 Priors. *Eur. Phys. J. C* **2025**, *85*, 488. [CrossRef]
22. Liu, T.; Li, X.; Xu, T.; Biesiada, M.; Wang, J. Torsion Cosmology in the Light of DESI, Supernovae and CMB Observational Constraints. *Eur. Phys. J. C* **2025**, *85*, 1351. [CrossRef]
23. Luongo, O.; Muccino, M. Model-Independent Cosmographic Constraints from DESI 2024. *Astron. Astrophys.* **2024**, *690*, A40. [CrossRef]

24. Loubser, S.I. Measuring the Expansion History of the Universe with DESI Cosmic Chronometers. *Mon. Not. R. Astron. Soc.* **2025**, *544*, 3064–3075. [CrossRef]
25. Nunes, R.C.; Pan, S.; Saridakis, E.N. New Constraints on Interacting Dark Energy from Cosmic Chronometers. *Phys. Rev. D* **2016**, *94*, 023508. [CrossRef]
26. Jimenez, R.; Moresco, M.; Verde, L.; Wandelt, B.D. Cosmic Chronometers with Photometry: A New Path to $H(z)$. *J. Cosmol. Astropart. Phys.* **2023**, *2023*, 047. [CrossRef]
27. Borghi, N.; Moresco, M.; Cimatti, A. Toward a Better Understanding of Cosmic Chronometers: A New Measurement of $H(z)$ at $z\sim0.7$. *Astrophys. J. Lett.* **2022**, *928*, L4. [CrossRef]
28. Bengaly, C.; Dantas, M.A.; Casarini, L.; Alcaniz, J. Measuring the Hubble Constant with Cosmic Chronometers: A Machine Learning Approach. *Eur. Phys. J. C* **2023**, *83*, 548. [CrossRef]
29. Wang, D. Pantheon+ Constraints on Dark Energy and Modified Gravity: An Evidence of Dynamical Dark Energy. *Phys. Rev. D* **2022**, *106*, 063515. [CrossRef]
30. Ballardini, M.; Finelli, F. Type Ia Supernovae Data with Scalar-Tensor Gravity. *Phys. Rev. D* **2022**, *106*, 063531. [CrossRef]
31. Maurya, D.C. Modified $f(Q, C)$ Gravity Dark Energy Models with Observational Constraints. *Mod. Phys. Lett. A* **2024**, *39*, 2450034. [CrossRef]
32. Abbott, D.C.T.M.C.; Acevedo, M.; Aguena, M.; Alarcon, A.; Allam, S.; Alves, O.; Amon, A.; Andrade-Oliveira, F.; Annis, J.; Armstrong, P.; et al. The Dark Energy Survey: Cosmology Results with ∼1500 New High-Redshift Type Ia Supernovae Using the Full 5 Yr Data Set. *Astrophys. J. Lett.* **2024**, *973*, L14. [CrossRef]
33. Chudaykin, A.; Kunz, M. Modified Gravity Interpretation of the Evolving Dark Energy in Light of DESI Data. *Phys. Rev. D* **2024**, *110*, 123524. [CrossRef]
34. Maluf, J.W. The Teleparallel Equivalent of General Relativity. *Ann. Phys.* **2013**, *525*, 339–357. [CrossRef]
35. Cai, Y.F.; Capozziello, S.; De Laurentis, M.; Saridakis, E.N. (T) Teleparallel Gravity and Cosmology. *Rep. Prog. Phys.* **2016**, *79*, 106901. [CrossRef] [PubMed]
36. Bahamonde, S.; Dialektopoulos, K.F.; Escamilla-Rivera, C.; Farrugia, G.; Gakis, V.; Hendry, M.; Hohmann, M.; Levi Said, J.; Mifsud, J.; Di Valentino, E. Teleparallel Gravity: From Theory to Cosmology. *Rep. Prog. Phys.* **2023**, *86*, 026901. [CrossRef]
37. Mishra, S.S.; Kolhatkar, A.; Sahoo, P.K. Big Bang Nucleosynthesis Constraints on $f(T, \mathcal{T})$ Gravity. *Phys. Lett. B* **2024**, *848*, 138391. [CrossRef]
38. Heinesen, A. Differential Age Observations and Their Constraining Power in Cosmology. *Phys. Rev. D* **2025**, *111*, 023539. [CrossRef]
39. Bhardwaj, V.K.; Dixit, A.; Rani, R.; Goswami, G.K.; Pradhan, A. An Axially Symmetric Transitioning Models with Observational Constraints. *Chin. J. Phys.* **2022**, *80*, 261–274. [CrossRef]
40. Adame, A.G.; Aguilar, J.; Ahlen, S.; Alam, S.; Alexander, D.M.; Alvarez, M.; Alves, O.; Anand, A.; Andrade, U.; Armengaud, E.; et al. DESI 2024 VI: Cosmological Constraints from the Measurements of Baryon Acoustic Oscillations. *J. Cosmol. Astropart. Phys.* **2025**, *2025*, 021. [CrossRef]
41. Brout, D.; Scolnic, D.; Popovic, B.; Riess, A.G.; Carr, A.; Zuntz, J.; Kessler, R.; Davis, T.M.; Hinton, S.; Jones, D.; et al. The Pantheon+ Analysis: Cosmological Constraints. *Astrophys. J.* **2022**, *938*, 110. [CrossRef]
42. Paliathanasis, A.; Leon, G. Cosmological Evolution in $f(T, B)$ Gravity. *Eur. Phys. J. Plus* **2021**, *136*, 1092. [CrossRef]
43. Franco, G.A.R.; Escamilla-Rivera, C.; Levi Said, J. Stability Analysis for Cosmological Models in $f(T, B)$ Gravity. *Eur. Phys. J. C* **2020**, *80*, 677. [CrossRef]
44. Mishra, S.S.; Mandal, S.; Sahoo, P.K. Constraining $f(T, \mathcal{T})$ Gravity with Gravitational Baryogenesis. *Phys. Lett. B* **2023**, *842*, 137959. [CrossRef]
45. Bahamonde, S.; Böhmer, C.G.; Wright, M. Modified Teleparallel Theories of Gravity. *Phys. Rev. D* **2015**, *92*, 104042. [CrossRef]